

Charge-induced electrochemical actuation of armchair carbon nanotube bundles

Nguyen T. Hung^{a,*}, Ahmad R. T. Nugraha^a, Riichiro Saito^a

^a*Department of Physics, Tohoku University, Sendai 980-8578, Japan*

Abstract

The effects of charge doping on the structural deformation and on the electronic structure of armchair single wall carbon nanotube (SWNT) bundles are investigated through first-principles calculations. In particular, we select a (6, 6) SWNT as an example and we calculate a mechanical deformation in the SWNT bundles as a function of gate voltage, which could serve as a basis of the electromechanical actuators in an artificial muscle. We find that the magnitudes of the actuation responses such as strain and stress of the (6, 6) SWNT bundle in the case of hole doping are substantially larger than those of electron doping. The (6, 6) SWNT bundle also exhibits a low-symmetry and opens an energy band gap of about 0.41 eV around the charge neutral condition, which allows a semiconductor-to-metal transition in the electron-doping regime when the relative shift of the Fermi energy goes up to 0.60 eV, above which the Young modulus increases.

1. Introduction

An artificial muscle is a novel actuator made of a variety of polymers or composites that change their shape when excited electrically. A composite of single wall carbon nanotubes (SWNTs) is known to be one of the strongest and stiffest materials [1, 2, 3], and they can reversibly contract and expand in volume under an applied voltage, similar to the natural muscle. Almost two decades ago, Baughman et al. [4, 5] had built an ultra-strong artificial muscle from bundles (or yarns) of SWNTs with electrochemical charging, in which the artificial muscle could generate force per unit area of about 26 MPa, which is almost 100 times larger than that of natural muscle (≈ 0.35 MPa) [6]. Therefore, the charge-induced electromechanical actuators of the SWNT bundles are not only fascinating from the scientific point of view but are also promising for technological applications. Gartstein et al. [7] analytically showed that the magnitude of the actuation response of semiconducting SWNTs could be substantially larger than that of graphite. On the other hand, Yin et al. [8] showed by first-principles calculation that carbon-carbon bond lengths of metallic SWNTs are changed by charge doping level, which lead to the modification of their electronic properties. While the artificial muscles in experiments were made of SWNT *bundles* (whose electronic structures show lower symmetry than those of the individual SWNTs), the theoretical descriptions for both the electronic structure and deformation under electromechanical charging so far are only available for *individual* SWNTs [7, 8, 9, 10].

A nanotube bundle consists of tens or several hundred individual SWNTs arranged in a hexagonal lattice of tubes and bound by the van der Waals force. A bundle containing many nanotubes with only one chirality is especially interesting because of its expected uniform response as an artificial muscle.

The chirality of a SWNT is defined by a set of integers (n, m) which specifies the geometrical structure of a SWNT and hence its physical properties [11]. With recent advances in the SWNT fabrication technique, armchair (n, n) and zigzag $(n, 0)$ SWNT bundles can be selectively synthesized [12, 13]. Moreover, separation and purification of SWNTs into single chirality level are now possible [14] and the alignment of SWNTs has also been realized [15]. Thus the computational design of artificial muscle will be important for obtaining the optimum artificial muscle. Note that although the formation of individual SWNTs into a bundle involves weak van der Waals interactions, their electronic properties can change significantly. For example, by a first principles calculation, Delaney et al. showed that a lowering symmetry of the armchair SWNT bundles caused by interactions between tubes induces a small energy band gap although the isolated armchair SWNTs are metallic tubes [16], which might affect the response of artificial muscle.

Among different SWNT structures, the armchair SWNTs are interesting to be studied for artificial muscle applications because of the two following reasons. First, an appropriate selection of the chirality of the (6, 6) armchair SWNTs could match the hexagonal lattice of the bundle which saves the computational time. Second, the armchair SWNTs are basically known to be metallic and the effect of the bundle formation on the SWNT electronic structure is more pronounced for metallic SWNTs, compared with semiconducting ones. Combining these two reasons, we could suggest the optimum structure for the artificial muscles. Furthermore, due to the weak tube-tube interactions, it is important to study the effects of electrochemical doping or gate voltage on the symmetry and on the electronic properties of the armchair SWNT bundles. However, many researchers often assumed in their calculation that the energy bands do not change by doping level and that only the Fermi energy is shifted by doping, which is known as the rigid band model [17, 18]. Even for isolated and individual SWNTs,

*Corresponding author. Tel.: +81 22 795 7754; Fax: +81 22 795 6447.

Email address: nguyen@flex.phys.tohoku.ac.jp (Nguyen T. Hung)

it is expected that the rigid band model is not suitable to consider the heavy doping of the metallic SWNTs [8], in which the lattice constant is modified.

In this paper, by considering the changes in the energy bands, we discuss the electromechanical properties of the armchair SWNT bundles as a function of charge doping, for both electron and hole doping cases. By first-principles calculation, we find two important physical phenomena in the doped armchair SWNT bundles, one is the semiconductor-metal transition in the armchair SWNT bundles as a result of heavy electron doping, and another one is a large change of strain by hole doping, which is essential in the artificial muscle applications. We expect that the armchair SWNT bundles can be strained by the doping due to the extremely high Young's modulus of individual SWNTs formed into the bundles [4]. For individual SWNTs and graphite, previous theoretical studies showed that an axial strain of about 1% might be achieved for both heavy electron and hole doping cases [19, 20]. Meanwhile, some previous experiments with the SWNT bundles showed that the largest strain is -1% when the negative potential is applied (hole-doped) and that the strain is very small ($\sim 0.02\%$) when the positive potential is applied (electron-doped) [21, 22], whose origin is not clear yet to our knowledge. In this work, we reproduce such an asymmetric behavior of the strain through the calculations of the strain, Young's modulus, and stress of the armchair SWNT bundles as a function of Fermi energy. We will show that the lengths of C-C bonds parallel and perpendicular to the bundle axis change differently for the hole doping and electron doping.

2. Calculation methods

To calculate the structural deformation variables (strain, Young's modulus, and stress) as a function of the Fermi energy, we define the relative shift of the Fermi energy, ΔE_F , for the charge (electron and hole) doping, which can be expressed by

$$\Delta E_F = E_F^{\text{neutral}} - E_F^{\text{doped}}, \quad (1)$$

where E_F^{neutral} and E_F^{doped} are the Fermi energy for a neutral and a charge doping, respectively. The Fermi energy is defined by the center of the energy gap for the semiconducting SWNT bundle case. In the case of the metallic SWNT bundle, in which the conduction and valence energy bands touch each other at the Dirac point, the Fermi energy is defined as the highest energy for occupied electrons. Note that equation (1) was already given in some earlier studies [8, 9], discussing the Fermi level dependence of optical transition energy and electronic properties in the SWNTs.

In this work, we choose the chirality $(n, m) = (6, 6)$ for a model calculation, which has the highest symmetry in the bundle, similar with that in the isolated SWNT. In Fig. 1(a) and (b), we show the perspective view of a bundle of $(6, 6)$ armchair SWNTs in three-dimensional space and its hexagonal unit cell including 24 carbon atoms, respectively. The periodic boundary conditions are applied for three dimensions. The simulation hexagonal unit cell dimensions are $a = b = d_t + d_i$ and c , where c (in Å) is the length of the unit vector along the tube axis, d_t

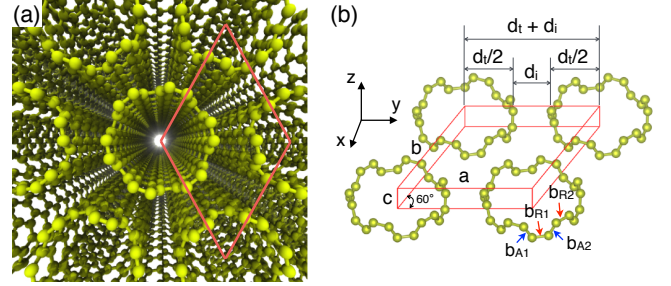


Figure 1: (a) Perspective view of the $(6, 6)$ armchair SWNT bundle in three-dimensional space. (b) Hexagonal unit cell of the $(6, 6)$ armchair SWNT bundle showing the lattice vector c along the tube axis, the diameter d_t , the intertube distance d_i , the C-C bonds perpendicular to the tube axis (b_{R1} and b_{R2}), and those parallel to the tube axis (b_{A1} and b_{A2}). Note that the box in (b) is a rhombus, thus the x -axis is not parallel to any edges of the box.

(in Å) is the diameter of the tube, and d_i (in Å) is the intertube distance as shown in Fig. 1(b).

We calculate the electronic properties of the $(6, 6)$ armchair SWNT bundles from first-principles by using Quantum ESPRESSO [23], which is a full density functional theory (DFT) simulation package using a plane-wave basis set [24, 25]. The Rabe-Rappe-Kaxiras-Joannopoulos ultrasoft pseudopotential with an energy cutoff of 60 Ry is chosen for the expansion of the plane waves [26]. The exchange-correlation energy is evaluated by the general-gradient approximation using the Perdew-Burke-Ernzerhof (PBE) function [27, 28], which is appropriate to model the interactions between the tubes in the bundle. We use a second version of the nonlocal van der Waals functional (vdW-DF2) [29]. Using vdW-DF2 is necessary to correctly capture the van der Waals interaction between the tubes in the bundle for obtaining the forces and the lattice parameters [30], which are important parameters for calculating the mechanical properties and electronic structure. In our simulation, the $8 \times 8 \times 24$ \mathbf{k} -point grids in the Brillouin-zone are used following the Monkhorst-Pack scheme, where \mathbf{k} is the electron wave vector [31].

To obtain the SWNT bundle structure, the atomic positions and cell vectors are fully relaxed by using the Broyden-Fletcher-Goldfarb-Shanno minimization method [32, 33, 34, 35]. This model is considered to be optimized when all the Hellmann-Feynman forces and all components of the stress are less than 5.0×10^{-4} Ry/a.u. and 5.0×10^{-2} GPa, respectively, which are adequate for the present purpose. In Fig. 1(b), we present scaled bond structures for the $(6, 6)$ SWNTs in the bundle without the charge doping, where $b_{R1} = b_{R2} = 1.427$ Å and $b_{A1} = b_{A2} = 1.428$ Å represent the C-C bonds perpendicular to and 30° from the tube axis, respectively. The tube orientation in the present model corresponds to the AB stacking in graphite [36]. It should be noted that in the case of $(6, 6)$ armchair SWNT bundle, the AB stacking configuration is more stable than the AA stacking configuration [30, 36].

For the energy band calculations, we used 100 \mathbf{k} points along the z -direction. To discuss the electromechanical actuation of the $(6, 6)$ armchair SWNT bundle with the charge doping level (ΔQ), ranging from $-0.9e$ to $+2.0e$ per unit cell, the electron

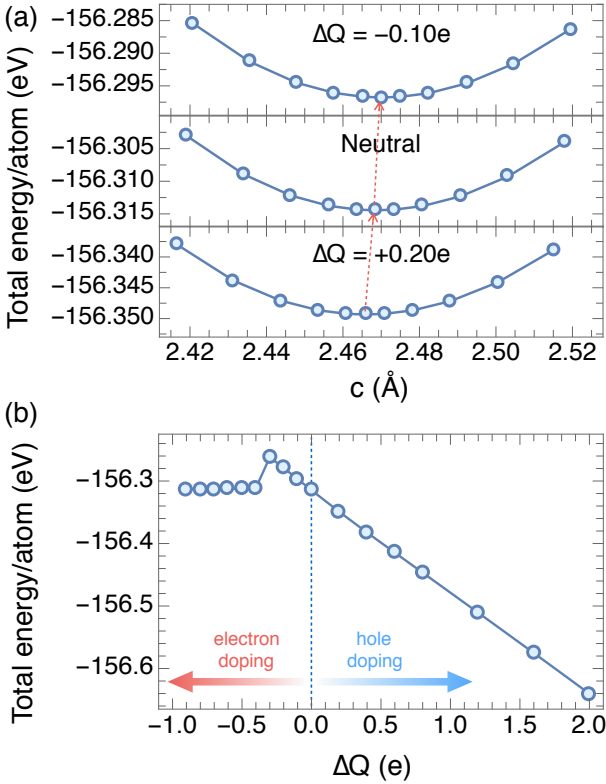


Figure 2: (a) Total energy per atom of the (6,6) armchair SWNT bundle unit cell plotted as a function of the lattice constant c . (b) Minimum total energy per atom of the (6,6) armchair SWNT bundle as a function of the charge (electron and hole) doping, with ΔQ ranging from $-0.9e$ to $+2.0e$ per unit cell.

(hole) doping is simulated by adding (removing) electrons to the SWNT bundle with the same amount of uniform positive (negative) charge in the background so as to keep the charge neutrality.

3. Results and discussion

3.1. Electronic structure of SWNT bundle

In Fig. 2(a), we show the total energy per atom of the (6,6) armchair SWNT bundle as a function of the lattice vector c ranging from 2.42 to 2.52 Å. As shown in Fig. 2(a), the local minimum total energy is observed at $c = 2.469$ Å in the neutral case which corresponds to the diameter $d_t = 8.226$ Å and the intertube distance $d_i = 3.258$ Å which is consistent with the previous reports [30, 36]. The scanning of the potential energy surfaces as a function of lattice constant are calculated for each charge (electron and hole) doping ΔQ . In Fig. 2(b), we show the minimum total energy per atom of the (6,6) armchair SWNT bundle as a function of ΔQ ranging from $-0.9e$ to $+2.0e$ per unit cell. Since we have 24 carbon atoms in the unit cell, $-0.1e$ ($+0.1e$) for electron (hole) doping corresponds to the added (removed) 0.004167 electron per carbon atom. The total energy monotonically decreases with increasing the hole doping. A similar trend with sharper slope is also found for the electron doping from $0.0e$ to $-0.3e$. However, the total energy becomes constant with further increase in the electron doping

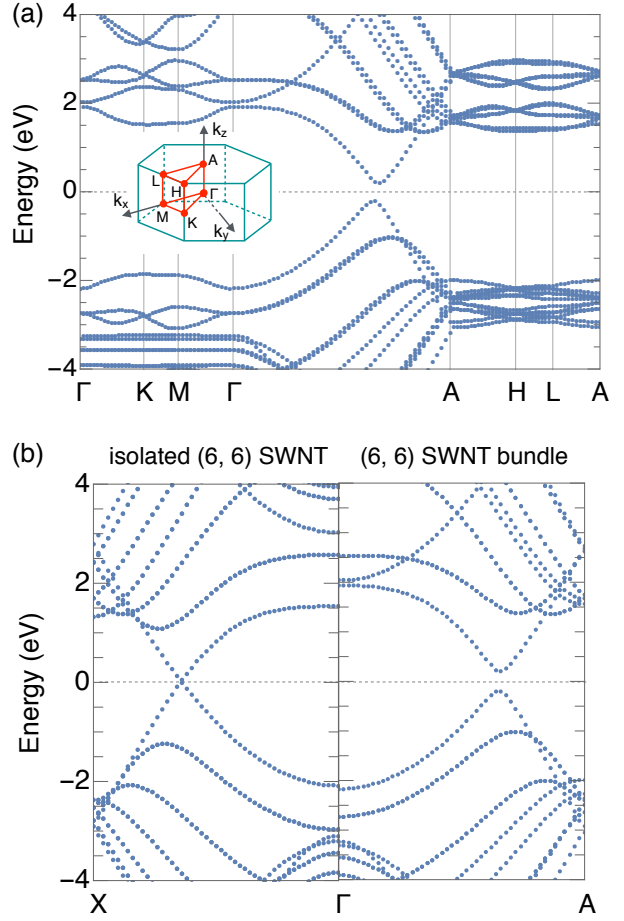


Figure 3: (a) Energy band structure along high-symmetry directions of the neutral (6,6) armchair SWNT bundle. Inset shows the high-symmetry points and lines in the corresponding Brillouin zone. (b) Energy band structure along Γ -X and Γ -A directions of the isolated (6,6) SWNT and the (6,6) SWNT bundle, respectively.

after a finite jump of total energy at $\Delta Q = -0.4e$. This suggests that the atomic structure of the bundle may be broken into individual SWNTs, which will be discussed later through intertube distance d_i calculations for heavy electron doping case.

Before discussing the optimized electronic structure of the (6,6) armchair SWNT bundle, it is worth mentioning the symmetry properties of individual armchair (n,n) SWNTs. The symmetry of an (n,n) SWNT is expressed by the direct product of the groups $D_n \otimes C_i$, where D_n consists of a vertical n -fold rotational axis C_n (parallel to the nanotube axis) and n horizontal 2-fold axes C_2 (perpendicular to the nanotube axis), and C_i consists of the identity E and inversion σ_i operators [37]. Since the symmetry operations $D_n \otimes C_i$ are described by the symmetry group D_{nh} or D_{nd} for even or odd n , respectively, an isolated individual (6,6) armchair SWNT with $n = 6$ has the D_{6h} symmetry. The structure of the bundle has a comparably high-symmetry if the individual nanotube and the bundle share all symmetry operations. Therefore, the (6,6) armchair SWNT bundle can have either the high-symmetry D_{6h} or the low-symmetry C_{6h} (loss of mirror planes) corresponding to the AA stacking or AB stacking in graphene, respectively [16, 30].

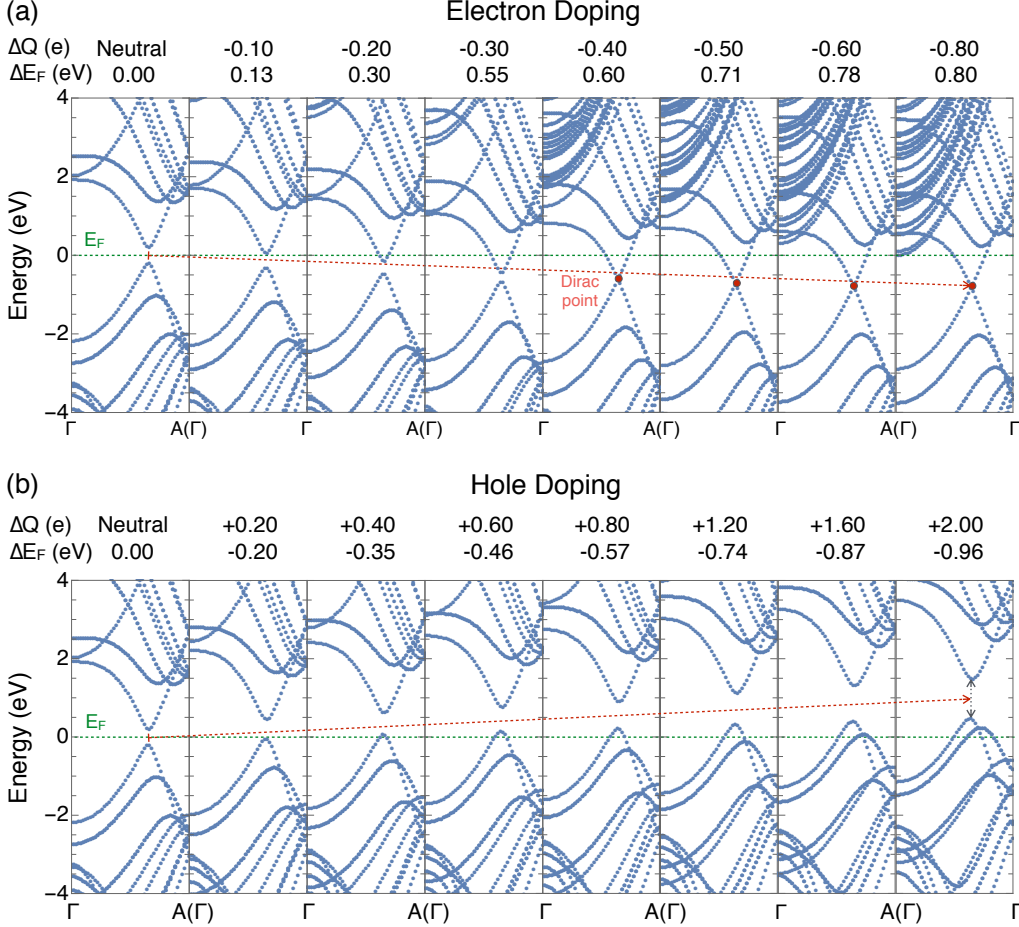


Figure 4: Energy band structures of the (6,6) armchair SWNT bundle with different (a) electron doping and (b) hole doping levels including those of the neutral (6,6) armchair SWNT bundle for comparison. The Fermi energy (straight dashed line) is set to zero for all plots. Dashed arrows are a guide for eyes to see the evolution of the Dirac point.

Since the AB stacking configuration is more stable than the AA stacking configuration [30, 36], we hereafter consider only the structure of the (6,6) armchair SWNT bundle with the AB stacking configuration with C_{6h} symmetry.

Figure 3(a) displays the energy band structure along the high-symmetry directions of the neutral (6,6) armchair SWNT bundle. The inset shows the symmetry points and lines in the corresponding Brillouin zone of the bundle. The lowering of symmetry from D_{6h} to C_{6h} leads to a band-gap opening in the bundle of armchair tubes [30, 16, 38]. As shown in Fig. 3(a), an energy band gap $E_g \approx 0.41$ eV opens up along the $\Gamma - A$ direction as a result of the low-symmetry C_{6h} in the (6,6) armchair SWNT bundle with the AB stacking configuration. This result reproduces a previous theoretical report of Ref. [30]. In Fig. 3(b), we compare the energy band structure an isolated (6,6) armchair SWNT with that of a neutral (6,6) armchair SWNT bundle considered in this work. Since the isolated (6,6) armchair SWNT has the high-symmetry D_{6h} , it shows a metallic behavior without the energy band gap. We note that the metal-like behavior is expected for the high-symmetry with AA-stacked configuration of the bundle [30, 38]. As we can see from Fig. 3(b), the valence and the conduction bands of the neutral (6,6) arm-

chair SWNT bundle are shifted upward and are more asymmetric compared with those of the isolated (6,6) armchair SWNT. The asymmetric distribution of the conduction and the valence bands originates from not only the effect of the overlap matrix element and the curvature-induced $\sigma - \pi$ hybridization [39], but also from the effect of the van der Waals interaction between the tubes in the bundle [30].

To study the variation of the electronic properties of the (6,6) armchair SWNT bundle with ΔQ , we have calculated the energy band structures of the (6,6) armchair SWNT bundle for all electron (hole) doping levels considered in the present work. Figures 4(a) and (b) show the energy band structures of the (6,6) armchair SWNT bundle under the electron and hole doping, respectively. As shown in Fig. 4(a), for the electron doping, the energy bands shift downward compared with the energy bands in the neutral case. The downward-shift gives $\Delta E_F > 0$. Since the downward-shift of the conduction bands is larger than that of the valence bands with decreasing ΔQ , the energy gap E_g decreases and eventually becomes a Dirac energy point at $\Delta Q = -0.40e$. Thus, the (6,6) armchair SWNT bundle becomes metallic at the electron doping at at $\Delta Q = -0.40e$. For further electron doping, the Dirac point slightly moves down-

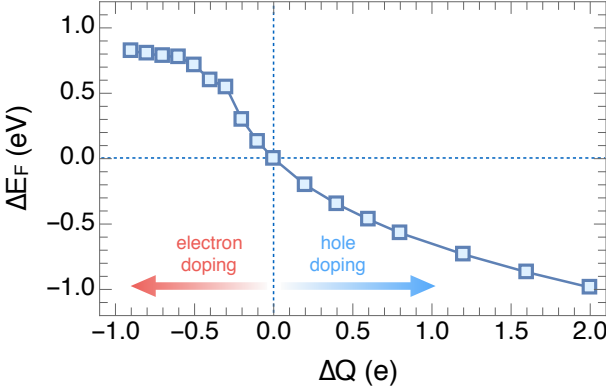


Figure 5: ΔE_F as a function of ΔQ for charge (electron and hole) doping.

ward to a lower energy position. In the case of hole doping, the energy bands of the (6, 6) armchair SWNT bundle shift upward by increasing ΔQ , as shown in Fig. 4(b), resulting in $\Delta E_F < 0$. The upward-shifts of the valence bands are smaller than those of the conduction bands with increasing ΔQ , which makes an increase of E_g for the hole doping. For heavy electron (hole) doping, the second conduction (valence) subband touches the Fermi energy which might change the transport properties of the SWNT bundle. We note that the asymmetric distribution of the conduction and the valence bands relative to the energy gap increases for both electron and hole doping cases.

As mentioned in the introduction, the rigid band model was commonly considered to investigate the effect of charge doping on the electronic structure of individual SWNTs or SWNT bundles [40, 41, 42]. In this model, the effective masses and band gaps are fixed, while the Fermi levels are shifted by charge doping. The applicability of the rigid band model was justified, for instance, in alkali- or nitrogen-doped SWNTs [41] and in the calculation of thermoelectric power of the semiconducting SWNTs [42]. However, in the case of heavy doping to obtain a high actuation, in which the Fermi energy can be changed up to 1 eV, the rigid band model is no longer suitable because the energy structure changes significantly. Therefore, in this work, we did not use the rigid band model, but utilized the altered band structures as they were obtained from the first-principles calculations.

In Fig. 5, we show ΔE_F as a function of ΔQ based on Eq. (1). In the neutral case, $\Delta E_F = 0$ from the definition in Eq. (1), while for the electron (hole) doping, ΔE_F monotonically decreases with increasing ΔQ . As we can see from Fig. 5, the change of ΔE_F with electron doping is larger than that with hole doping because of an asymmetry of energy bands (see in Fig. 4). For the heavy electron (hole) doping, the higher energy valence bands around the Γ point show smaller downward (upward)-shift, resulting in a smaller increase (decrease) of ΔE_F . In the electron (hole) doping, ΔQ of $-1.0e$ ($+2.0e$) per unit cell corresponds to the addition of 0.04167 (removal of 0.08334) electron per carbon atom, which is appropriate for our calculation because the limit of the experimentally accessible charge is from about -0.3 to $+0.1$ electron per carbon atom for graphite [20]. In Fig. 6, we plot the energy gap E_g of the (6, 6)

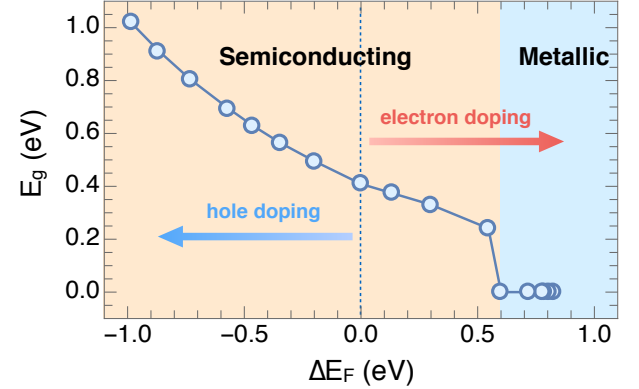


Figure 6: Energy band gaps of the (6, 6) armchair SWNT bundle as a function of ΔE_F . The apricot and light blue shadings indicate the regime in which the (6, 6) armchair SWNT bundle has semiconducting and metallic states, respectively.

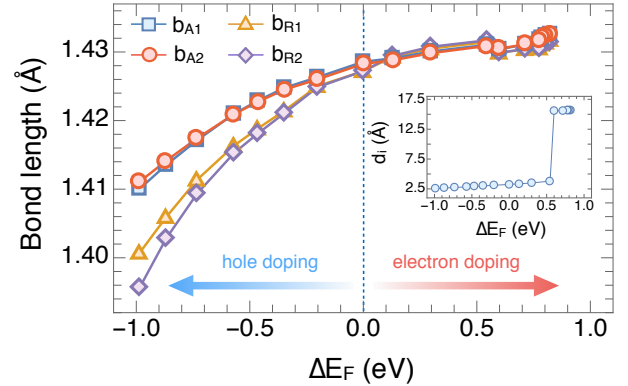


Figure 7: C-C bond lengths b_{A1} , b_{A2} , b_{R1} , and b_{R2} as a function of ΔE_F . Insert shows the intertube distance d_i as a function of ΔE_F .

armchair SWNT bundle as a function of ΔE_F . In the neutral case, the (6, 6) armchair SWNT bundle is semiconducting with $E_g = 0.41$ eV. For the electron (hole) doping, E_g decrease (increase) with increasing (decreasing) ΔE_F . This result suggests that the energy band gap of the (6, 6) armchair SWNT bundle is tunable by changing the Fermi energy, which can be achieved experimentally by electrochemical doping or by applying a gate voltage. As shown in Fig. 6, a semiconductor-metal transition occurs in the (6, 6) SWNT bundle when ΔE_F is adjusted up to 0.60 eV. The reason for this transition will be discussed below in terms of the C-C bond length, which is also related with the symmetry properties of the (6, 6) armchair SWNT bundle as a function of ΔE_F .

3.2. Mechanical deformation

In Fig. 7, we plot the C-C bond lengths of b_{A1} , b_{A2} , b_{R1} , and b_{R2} [defined in Fig. 1(b)] as a function of ΔE_F . The inset shows the intertube distance d_i as a function of ΔE_F . The (6, 6) armchair SWNT bundle has the C_{6h} symmetry, thereby we consider all different bond length variables (b_{A1} , b_{A2} , b_{R1} and b_{R2}) in one sixth of the bundle (totally 24 C-C bond lengths). In the neutral case at $\Delta E_F = 0$, we have $b_{A1} = b_{A2} = 1.428$ Å and $b_{R1} = b_{R2} = 1.427$ Å which are larger than the bond lengths of the isolated (6, 6) armchair SWNT ($b_{A1} = b_{A2} = 1.425$ Å

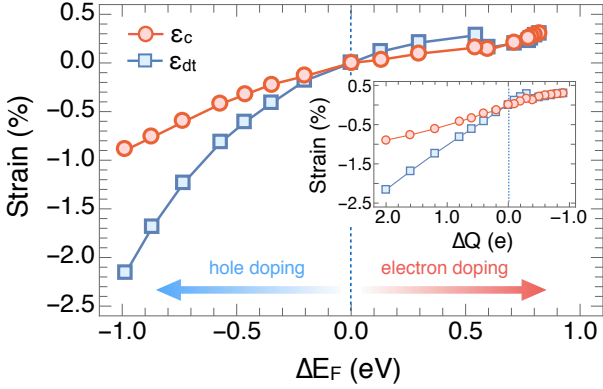


Figure 8: Strain of length (ϵ_c) and strain of diameter (ϵ_{dt}) plotted as function of ΔE_F . Inset gives the strain versus the charge doping.

and $b_{R1} = b_{R2} = 1.424 \text{ \AA}$). It has been reported that in the isolated armchair tubes, the bonds parallel to the tube axis b_A are longer than those perpendicular to the tube axis b_R due to the curvature effect of the tubes [3, 43]. For the electron doping, b_{A1}, b_{A2}, b_{R1} and b_{R2} increase by increasing ΔE_F up to 0.60 eV. The difference between bond lengths are not significant for $\Delta E_F > 0$. As we can see from the inset of Fig. 7, since the intertube distance suddenly increases at $\Delta E_F = 0.60 \text{ eV}$ under the heavy electron doping, making a failure of the structure of the bundle with the absence of the van der Waals interaction. In fact, the structure of the electron-doped (6, 6) armchair SWNT bundle for $\Delta E_F \geq 0.60 \text{ eV}$ has higher symmetry (D_{6h}) than that of the neutral one (C_{6h}), which leads to decrease of E_g under the electron doping (see in Fig. 6).

In order to study the variation of the structural deformation as a function of Fermi energy, we define the strain as

$$\varepsilon_x = \Delta x / x_0, \quad (2)$$

where x_0 is either the length c or diameter d_t of the SWNT in the unit cell of bundle at geometry optimization for neutral case, as shown in Fig. 1(b), and Δx is the increment of the length Δc or diameter Δd_t under the charge doping level. In Fig. 8 we plot the strain of length ε_c and diameter ε_{dt} of the (6, 6) armchair SWNT bundle as function of ΔE_F . In the neutral case, we obtain $\varepsilon_c = \varepsilon_{dt} = 0$, while for the electron (hole) doping, ε_c and ε_{dt} increase (decrease) with increasing (decreasing) ΔE_F . In the doped SWNT bundles, the increase of ε_c and ε_{dt} with the electron doping is smaller than the decrease of ε_c and ε_{dt} with the hole doping. As shown in the inset of Fig. 8, ε_c and ε_{dt} are approximately a linear function of ΔQ but are nonlinear with respect to ΔE_F . At hole doping $\Delta Q = +2.0e$ (removed ~ 0.08 electron per carbon atom), $\varepsilon_c \sim -1\%$ is larger than that of individual (6, 6) SWNTs ($\varepsilon_c \sim -0.7\%$ at $\Delta Q = +2.0e$) [20]. It is important to note that the strain of the SWNT bundle in Fig. 8 shows an asymmetric behavior with respect to the doping level, indicated by a higher (smaller) strain under heavy hole (electron) doping. On the other hand, the strain of the individual SWNT exhibits a symmetric shape with nearly the same strain under both electron and hole dopings [8, 20]. Recently, the influence of the gate voltage on the structural deformation in

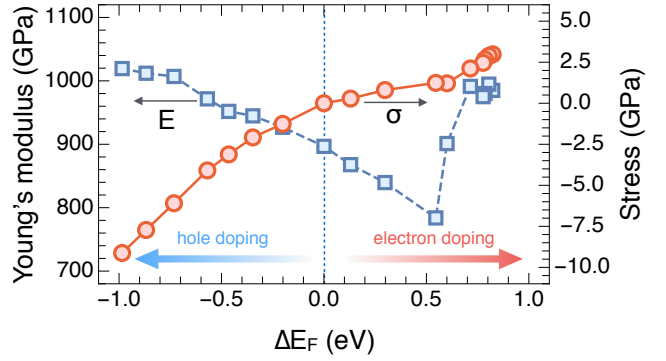


Figure 9: Young's modulus (E) and stress (σ) as function of ΔE_F .

both multiwall carbon nanotube (MWNT) bundles (or yarns) and SWNT bundles have been studied experimentally by using electrochemical doping [22, 21, 4, 44]. In these experiments, the largest strain obtained is nearly -1% with the applied potential of about -1V (hole-doped), while the strain is quite small with the applied potential of about $+1\text{V}$ (electron-doped) [22]. This asymmetrical behavior of the actuation strain is in good agreement with our present calculation. It should be noted that the strain range of natural muscles is very high (up to 20% [6]) compared with that of SWNT bundles ($\sim 1\%$). Therefore, a possible approach to obtain carbon nanotube bundle actuators is by fabricating bundle networks from a forest of multi-walled carbon nanotubes, which could yield strain as high as 220% and strain rate of about $3.7 \times 10^4\%$ per second [45].

Finally, to study the Young modulus as a function of Fermi energy, the SWNT bundle is initially relaxed to its minimum total energy with the lattice vector c along the axis for each ΔQ [see again Fig. 2(a)]. We then apply a series of small tensile strains ($\pm 0.2\%, \pm 0.5\%, \pm 0.9\%, \pm 1.4\%, \pm 2\%$) on the unit cell and simultaneously relax the other stress components to zero (Poisson's ratio contraction under uniaxial tension). Since the system stays in the harmonic regime with the small strains, total energy values can be fitted to a polynomial of strain. Then, we obtain the Young modulus E from the strain derivatives of the polynomial for each charge doping level, which is defined by

$$E = \frac{1}{V_0} \left. \frac{\partial^2 U(\varepsilon)}{\partial \varepsilon^2} \right|_{\varepsilon=0}, \quad (3)$$

with

$$U(\varepsilon) = U_0 + \frac{\partial U(\varepsilon)}{\partial \varepsilon} \varepsilon + \frac{1}{2} \frac{\partial U^2(\varepsilon)}{\partial \varepsilon^2} \varepsilon^2 + \dots, \quad (4)$$

where $U(\varepsilon)$, U_0 , V_0 , and ε are the strain energy, the total energy at equilibrium, the volume at equilibrium, and the tensile strain for each ΔQ , respectively. To obtain V_0 , we use the constant thickness of a SWNT ($d_0 = 3.4 \text{ \AA}$) in the bundle [3, 46], in which d_0 is assumed to be independent of the small strain and ΔQ . It is important to know how much force per cross-sectional area (also known as stress) is generated by the charge doping level. For small strain, the axial stress can be described as $\sigma = \varepsilon_c E$, where ε_c is the axial strain as a function of ΔE_F [see in Fig. 8] and E is the Young modulus [Eq. 3].

Figure 9 displays the Young modulus E and the axial stress σ as a function of ΔE_F . In the neutral case, the strength of the (6, 6) SWNT bundle ($E = 897$ GPa) is weaker than that of the isolated (6, 6) SWNT ($E = 978$ GPa [3]) because the bond lengths of the bundle are only changed a little under the van der Waals forces between the tubes in the bundle, as shown in Fig. 7. For the electron doping case, E decreases with increasing ΔE_F up to 0.60 eV. Since the structure of the bundle is broken for heavy electron doping, the strength of the (6, 6) SWNT bundle is comparable to that of the isolated (6, 6) SWNT with $\Delta E_F \geq 0.60$ eV. For the hole doping case, E increases with decreasing ΔE_F because the bundle is in a state of compression. Large strain and large Young's modulus lead to large stress, $\sigma \approx -9$ GPa (26000 times the natural muscle), that is generated by heavy doping level at $\Delta E_F \approx -1$ eV. For heavy electron doping, we obtain $\sigma \approx 3$ GPa, weaker than in the case of hole doping. Our results suggest that the hole doping should be good for the artificial muscle application of the SWNT bundle.

4. Conclusions

We have performed a first principles theoretical study on the structural deformation and on the electronic structure as a function of the Fermi energy for armchair SWNT bundles. The results obtained reveal that the (6, 6) armchair SWNT bundle is semiconducting with energy band gap of about 0.41 eV around the charge neutral condition due to their low-symmetry. The electronic properties of a (6, 6) armchair SWNT bundle strongly depend on the Fermi energy. The Fermi-energy-dependent electronic properties give a semiconductor-metal transition in the bundle as a result of heavy electron doping when the relative shift of the Fermi energy is adjusted up to 0.60 eV. Moreover, the lengths of the C-C bonds parallel and perpendicular to the bundle axis also depend on the Fermi energy, resulting in the observed asymmetry of the strain-Fermi energy curves. For heavy hole doping, the strains of length and diameter can be achieved up to 1% and 2%, respectively, while the structure of the bundle is broken for heavy electron doping. Because of large strain and large Young's modulus, the stress generated by heavy hole doping is larger than that by heavy electron doping. This study gives a theoretical support for the actuation response of the carbon nanotube bundles that are tunable by the charge doping level.

Acknowledgements

N.T.H. and A.R.T.N acknowledge the Interdepartmental Doctoral Degree Program for Multidimensional Materials Science Leaders in Tohoku University. R.S. acknowledges JSPS KAKENHI Grant Numbers JP25107005 and JP25286005.

References

- [1] M. F. Yu, O. Lourie, M. J. Dyer, K. Moloni, T. F. Kelly, R. S. Ruoff, Strength and breaking mechanism of multiwalled carbon nanotubes under tensile load, *Science* 287 (2000) 637–640.
- [2] M. F. Yu, B. S. Files, S. Arepalli, R. S. Ruoff, Tensile loading of ropes of single wall carbon nanotubes and their mechanical properties, *Phys. Rev. Lett.* 84 (2000) 5552.
- [3] N. T. Hung, D. V. Truong, V. V. Thanh, R. Saito, Intrinsic strength and failure behaviors of ultra-small single-walled carbon nanotubes, *Comput. Mater. Sci.* 114 (2016) 167–171.
- [4] R. H. Baughman, C. Cui, A. A. Zakhidov, Z. Iqbal, J. N. Barisci, G. M. Spinks, G. G. Wallace, A. Mazzoldi, D. De Rossi, A. G. Rinzler, O. Jaschinski, S. Roth, M. Kertesz, Carbon nanotube actuators, *Science* 284 (1999) 1340–1344.
- [5] R. H. Baughman, A. A. Zakhidov, W. A. de Heer, Carbon nanotubes—the route toward applications, *Science* 297 (2002) 787–792.
- [6] J. D. W. Madden, N. A. Vandesteeg, P. A. Anquetil, P. G. A. Madden, A. Takshi, R. Z. Pytel, S. R. Lafontaine, P. A. Wieringa, I. W. Hunter, Artificial muscle technology: physical principles and naval prospects, *IEEE J. Oceanic Eng.* 29 (2004) 706–728.
- [7] Y. N. Gartstein, A. A. Zakhidov, R. H. Baughman, Charge-induced anisotropic distortions of semiconducting and metallic carbon nanotubes, *Phys. Rev. Lett.* 89 (2002) 045503.
- [8] L. C. Yin, H. M. Cheng, R. Saito, M. S. Dresselhaus, Fermi level dependent optical transition energy in metallic single-walled carbon nanotubes, *Carbon* 49 (2011) 4774–4780.
- [9] L. C. Yin, R. Saito, M. S. Dresselhaus, The fermi level dependent electronic properties of the smallest (2, 2) carbon nanotube, *Nano. Lett.* 10 (2010) 3290–3296.
- [10] C. Li, T. W. Chou, Theoretical studies on the charge-induced failure of single-walled carbon nanotubes, *Carbon* 45 (2007) 922–930.
- [11] R. Saito, M. Fujita, G. Dresselhaus, M. S. Dresselhaus, Electronic structures of carbon tubules based on C_{60} , *Phys. Rev. B* 46 (1992) 1804–1811.
- [12] C. Blum, N. Sturzl, F. Hennrich, S. Lebedkin, S. Heeg, H. Dumlich, S. Reich, M. M. Kappes, Selective bundling of zigzag single-walled carbon nanotubes, *ACS Nano* 5 (2011) 2847–2854.
- [13] E. H. Hároz, W. D. Rice, B. Y. Lu, S. Ghosh, R. H. Hauge, R. B. Weisman, S. K. Doorn, J. Kono, Enrichment of armchair carbon nanotubes via density gradient ultracentrifugation: Raman spectroscopy evidence, *ACS Nano* 4 (2010) 1955–1962.
- [14] H. Liu, D. Nishide, T. Tanaka, H. Kataura, Large-scale single-chirality separation of single-wall carbon nanotubes by simple gel chromatography, *Nat. Commun.* 2 (2011) 309.
- [15] J. Shaver, A. N. G. Parra-Vasquez, S. Hansel, O. Portugall, C. H. Mielke, M. Von Ortenberg, R. H. Hauge, M. Pasquali, J. Kono, Alignment dynamics of single-walled carbon nanotubes in pulsed ultrahigh magnetic fields, *ACS Nano* 3 (2008) 131–138.
- [16] P. Delaney, H. J. Choi, J. Ihm, S. G. Louie, M. L. Cohen, Broken symmetry and pseudogaps in ropes of carbon nanotubes, *Nature* 391 (1998) 466–468.
- [17] M. H. R. Lankhorst, H. J. M. Bouwmeester, H. Verweij, Use of the rigid band formalism to interpret the relationship between o chemical potential and electron concentration in $La_{1-x}Sr_xCoO_{3-\delta}$, *Phys. Rev. Lett.* 77 (1996) 2989–2992.
- [18] A. H. Marshak, C. M. V. Vliet, Electrical current and carrier density in degenerate materials with nonuniform band structure, *Proceedings of the IEEE* 72 (1984) 148–164.
- [19] T. Mirfakhrai, R. Krishna-Prasad, A. Nojeh, J. D. W. Madden, Electromechanical actuation of single-walled carbon nanotubes: an ab initio study, *Nanotechnology* 19 (2008) 315706.
- [20] G. Sun, J. Kürti, M. Kertesz, R. H. Baughman, Dimensional changes as a function of charge injection in single-walled carbon nanotubes, *J. Am. Chem. Soc.* 124 (2002) 15076–15080.
- [21] T. Mirfakhrai, J. Oh, M. Kozlov, E. C. W. Fok, M. Zhang, S. Fang, R. H. Baughman, J. D. W. Madden, Electrochemical actuation of carbon nanotube yarns, *Smart Mater. Struct.* 16 (2007) S243.
- [22] J. Foroughi, G. M. Spinks, G. G. Wallace, J. Oh, M. E. Kozlov, S. Fang, T. Mirfakhrai, J. D. W. Madden, M. K. Shin, S. J. Kim, R. H. Baughman, Torsional carbon nanotube artificial muscles, *Science* 334 (2011) 494–497.
- [23] P. Giannozzi, S. Baroni, N. Bonini, M. Calandra, R. Car, C. Cavazzoni, D. Ceresoli, G. L. Chiarotti, M. Cococcioni, I. Dabo, A. D. Corso, S. d. Gironcoli, S. Fabris, G. Fratesi, R. Gebauer, U. Gerstmann, C. Gougousis, A. Kokalj, M. Lazzeri, L. Martin-Samos, N. Marzari, F. Mauri,

- R. Mazzarello, S. Paolini, A. Pasquarello, L. Paulatto, C. Sbraccia, S. Scandolo, G. Sclauzero, A. P. Seitsonen, A. Smogunov, P. Umari, R. M. Wentzcovitch, Quantum espresso: a modular and open-source software project for quantum simulations of materials, *J. Phys. Condens. Matter* 21 (2009) 395502.
- [24] P. Hohenberg, W. Kohn, Inhomogeneous electron gas, *Phys. Rev.* 136 (1964) B864.
- [25] W. Kohn, L. J. Sham, Self-consistent equations including exchange and correlation effects, *Phys. Rev.* 140 (1965) A1133.
- [26] A. M. Rappe, K. M. Rabe, E. Kaxiras, J. D. Joannopoulos, Optimized pseudopotentials, *Phys. Rev. B* 41 (1990) 1227.
- [27] We used the pseudopotentials from <http://www.quantum-espresso.org>.
- [28] J. P. Perdew, K. Burke, M. Ernzerhof, Generalized gradient approximation made simple, *Phys. Rev. Lett.* 77 (1996) 3865.
- [29] T. Thonhauser, V. R. Cooper, S. Li, A. Puzder, P. Hyldgaard, D. C. Langreth, Van der waals density functional: Self-consistent potential and the nature of the van der waals bond, *Phys. Rev. B* 76 (2007) 125112.
- [30] H. Dumlich, S. Reich, Nanotube bundles and tube-tube orientation: A van der waals density functional study, *Phys. Rev. B* 84 (2011) 064121.
- [31] H. J. Monkhorst, J. D. Pack, Special points for brillouin-zone integrations, *Phys. Rev. B* 13 (1976) 5188.
- [32] C. G. Broyden, The convergence of a class of double-rank minimization algorithms 1. general considerations, *IMA J. Appl. Math.* 6 (1970) 76–90.
- [33] R. Fletcher, A new approach to variable metric algorithms, *Comput. J.* 13 (1970) 317–322.
- [34] D. Goldfarb, A family of variable-metric methods derived by variational means, *Math. Comput.* 24 (1970) 23–26.
- [35] D. F. Shanno, Conditioning of quasi-newton methods for function minimization, *Math. Comput.* 24 (1970) 647–656.
- [36] S. Okada, A. Oshiyama, S. Saito, Pressure and orientation effects on the electronic structure of carbon nanotube bundles, *J. Phys. Soc. Jpn.* 70 (2001) 2345–2352.
- [37] R. Saito, G. Dresselhaus, M. S. Dresselhaus, *Physical Properties of Carbon Nanotubes*, World Scientific, 1998.
- [38] S. Reich, C. Thomsen, P. Ordejón, Electronic band structure of isolated and bundled carbon nanotubes, *Phys. Rev. B* 65 (2002) 155411.
- [39] P. M. Ajayan, Nanotubes from carbon, *Chem. Rev.* 99 (1999) 1787.
- [40] S. Okada, A. Oshiyama, S. Susumu, Nearly free electron states in carbon nanotube bundles, *Phys. Rev. B* 62 (2000) 7634.
- [41] P. Ajayan, R. Arenal, M. Rümmeli, A. Rubio, P. Pichler, The doping of carbon nanotubes with nitrogen and their potential applications, *Carbon* 99 (2010) 575–586.
- [42] N. T. Hung, A. R. T. Nugraha, E. H. Hasdeo, M. S. Dresselhaus, R. Saito, Diameter dependence of thermoelectric power of semiconducting carbon nanotubes, *Phys. Rev. B* 92 (2015) 165426.
- [43] Y. Akai, S. Saito, Electronic structure, energetics and geometric structure of carbon nanotubes: A density-functional study, *Physica E* 29 (2005) 555–559.
- [44] Y. Shang, X. He, C. Wang, L. Zhu, Q. Peng, E. Shi, S. Wu, Y. Yang, W. Xu, R. Wang, S. Du, A. Cao, Y. Li, Large-deformation, multifunctional artificial muscles based on single-walled carbon nanotube yarns, *Adv. Eng. Mater.* 17 (2015) 14–20.
- [45] A. E. Aliev, J. Oh, M. E. Kozlov, A. A. Kuznetsov, S. Fang, A. F. Fonseca, R. Ovalle, M. D. Lima, M. H. Haque, Y. N. Gartstein, M. Zhang, A. A. Zakhidov, R. H. Baughman, Giant-stroke, superelastic carbon nanotube aerogel muscles, *Science* 323 (2009) 1575–1578.
- [46] P. G. Collins, M. S. Arnold, P. Avouris, Engineering carbon nanotubes and nanotube circuits using electrical breakdown, *Science* 292 (2001) 706–709.